A self-coherent receiver for detection of PolMUX coherent signals

Jingshi Li,[1,*] Rene Schmogrow,[1] David Hillerkuss,[1] Philipp C. Schindler,[1] Moshe Nazarathy,[3] Carsten Schmidt-Langhorst,[4] Shalva-Ben Ezra,[5] Igor Tselniker,[3] Christian Koos,[1,2] Wolfgang Freude,[1,2] and Juerg Leuthold[1,2]

[1]*Institute of Photonics and Quantum Electronics, Karlsruhe Institute of Technology, 76131 Karlsruhe, Germany*
[2]*Institute of Microstructure Technology (IMT), Karlsruhe Institute of Technology (KIT), 76344 Karlsruhe, Germany*
[3]*Electrical Engineering Department, Technion, Israel Institute of Technology, Haifa, 32000, Israel*
[4]*Fraunhofer Institute for Telecommunications, Heinrich-Hertz-Institut, Einsteinufer 37, 10587 Berlin, Germany*
[5]*Finisar Corporation, Nes Ziona, Israel*
[*]*jingshi.li@kit.edu*

Abstract: A self-coherent receiver capable of demultiplexing PolMUX-signals without an external polarization controller is presented. Training sequences are introduced to estimate the polarization rotation, and a decision feedback recursive algorithm mitigates the random walk of the recovered field. The concept is tested for a PolMUX-DQPSK modulation format where one polarization carries a normal DQPSK signal while the other polarization is encoded as a progressive phase-shift DQPSK signal. An experimental demonstration of the scheme for a 112 Gbit/s PolMUX-DQPSK signal is presented.

OCIS codes: (060.1660) Coherent communications; (060.5060) Phase modulation; (060.2330) Fiber optics communication.

References and links

1. C. R. S. Fludger, T. Duthel, D. Van den Borne, C. Schulien, E. D. Schmidt, T. Wuth, J. Geyer, E. De Man, Khoe Giok-Djan, and H. de Waardt, "Coherent equalization and POLMUX-RZ-DQPSK for robust 100-GE transmission," J. Lightwave Technol. **26**(1), 64–72 (2008).
2. X. Liu, S. Chandrasekhar, and A. Leven, "Digital self-coherent detection," Opt. Express **16**(2), 792–803 (2008).
3. N. Kikuchi, K. Mandai, K. Sekine, and S. Sasaki, "Incoherent 32-level optical multilevel signaling technologies," J. Lightwave Technol. **26**(1), 150–157 (2008).
4. J. Zhao, M. E. McCarthy, and A. D. Ellis, "Electronic dispersion compensation using full optical-field reconstruction in 10Gbit/s OOK based systems," Opt. Express **16**(20), 15353–15365 (2008).
5. J. Li, K. Worms, P. Vorreau, D. Hillerkuss, A. Ludwig, R. Maestle, S. Schuele, U. Hollenbach, J. Mohr, W. Freude, and J. Leuthold, "Optical vector signal analyzer based on differential direct detection," in Proc. of IEEE Photonics Society (LEOS Annual Meeting) 2009 (Belek-Antalya, Turkey), Paper TuA4 (2009).
6. J. Li, K. Worms, R. Maestle, D. Hillerkuss, W. Freude, and J. Leuthold, "Free-space optical delay interferometer with tunable delay and phase," Opt. Express **19**(12), 11654–11666 (2011).
7. J. Li, C. Schmidt-Langhorst, R. Schmogrow, D. Hillerkuss, M. Lauermann, M. Winter, K. Worms, C. Schubert, C. Koos, W. Freude, and J. Leuthold, "Self-coherent receiver for PolMUX coherent signals," in Proc. Optical Fiber Commun. Conf. (OFC)/Natl. Fiber Optic Eng. Conf. (NFOEC), paper OWV5 (2011).
8. I. Tselniker, M. Nazarathy, S.-B. Ezra, J. Li, and J. Leuthold, "Self-coherent complex field reconstruction with in-phase and quadrature delay detection without a direct-detection branch," Opt. Express **20**(14), 15452–15473 (2012).
9. J. M. Kahn and K.-P. Ho, "Spectral efficiency limits and modulation/detection techniques for DWDM systems," IEEE J. Sel. Top. Quantum Electron. **10**(2), 259–272 (2004).
10. D. van den Borne, S. Jansen, G. Khoe, H. de Wardt, S. Calabro, and E. Gottwald, "Differential quadrature phase shift keying with close to homodyne performance based on multi-symbol phase estimation," IEE Seminar on Optical Fiber Comm. and Electronic Signal Processing, ref. No. 2005–11310 (2005).
11. D. van den Borne, S. L. Jansen, E. Gottwald, P. M. Krummrich, G. D. Khoe, and H. de Waardt, "1.6-b/s/Hz spectrally efficient transmission over 1700 km of SSMF using 40 × 85.6-Gb/s POLMUX-RZ-DQPSK," J. Lightwave Technol. **25**(1), 222–232 (2007).
12. A. Gnauck, G. Charlet, P. Tran, P. Winzer, C. Doerr, J. Centanni, E. Burrows, T. Kawanishi, T. Sakamoto, and K. Higuma, "25.6-Tb/s WDM transmission of polarization-multiplexed RZ-DQPSK signals," J. Lightwave Technol. **26**(1), 79–84 (2008).

#172813 - $15.00 USD Received 17 Jul 2012; revised 20 Aug 2012; accepted 21 Aug 2012; published 4 Sep 2012

13. M. Yagi, S. Satomi, and S. Ryu, "Field trial of 160-Gb/s, polarization-division multiplexed RZ-DQPSK transmission system using automatic polarization control," in Proc. Optical Fiber Commun. Conf. (OFC)/Natl. Fiber Optic Eng. Conf. (NFOEC), Feb. 2008, paper OTuT7 (2008).
14. B. Koch, R. Noé, V. Mirvoda, D. Sandel, V. Filsinger, and K. Puntsri, "40-krad/s polarization tracking in 200-Gb/s PDM-RZ-DQPSK transmission over 430 km," IEEE Photon. Technol. Lett. **22**(9), 613–615 (2010).
15. C. R. Doerr and L. Chen, "Monolithic PDM-DQPSK receiver in silicon," in Proc. of Eur. Conf. Optical Communication (ECOC 2010), Paper PD3.6 (2010).
16. S. Chandrasekhar, X. Liu, A. Konczykowska, F. Jorge, J. Dupuy, and J. Godin, "Direct detection of 107-Gb/s polarization-multiplexed RZ-DQPSK without optical polarization demultiplexing," IEEE Photon. Technol. Lett. **20**(22), 1878–1880 (2008).
17. R. Nagarajan, J. Rahn, M. Kato, J. Pleumeekers, D. Lambert, V. Lal, H.-S. Tsai, A. Nilsson, A. Dentai, M. Kuntz, R. Malendevich, J. Tang, J. Zhang, T. Butrie, M. Raburn, B. Little, W. Chen, G. Goldfarb, V. Dominic, B. Taylor, M. Reffle, F. Kish, and D. Welch, "10 Channel, 45.6 Gb/s per Channel, polarization-multiplexed DQPSK, InP receiver photonic integrated circuit," J. Lightwave Technol. **29**(4), 386–395 (2011).
18. S. J. Savory, "Digital filters for coherent optical receivers," Opt. Express **16**(2), 804–817 (2008).
19. C. R. Doerr, D. M. Gill, A. H. Gnauck, L. L. Buhl, P. J. Winzer, M. A. Cappuzzo, A. Wong-Foy, E. Y. Chen, and L. T. Gomez, "Monolithic demodulator for 40-Gbs DQPSK using a star coupler," J. Lightwave Technol. **24**(1), 171–174 (2006).
20. L. Zimmermann, K. Voigt, G. Winzer, K. Petermann, and C. M. Weinert, "C-band optical 90° hybrids based on Silicon-on insulator 4×4 waveguide coupler," IEEE Photon. Technol. Lett. **21**(3), 143–145 (2009).
21. N. Sigron, I. Tselniker, and M. Nazarathy, "Carrier phase estimation for optically coherent QPSK based on Wiener-optimal and adaptive Multi-Symbol Delay Detection (MSDD)," Opt. Express **20**(3), 1981–2003 (2012).
22. X. Wei, A. H. Gnauck, D. M. Gill, X. Liu, U.-V. Koc, S. Chandrasekhar, G. Raybon, and J. Leuthold, "Optical pi/2-DPSK and its tolerance to filtering and polarization-mode dispersion," IEEE Photon. Technol. Lett. **15**(11), 1639–1641 (2003).
23. R. Schmogrow, D. Hillerkuss, M. Dreschmann, M. Huebner, M. Winter, J. Meyer, B. Nebendahl, C. Koos, J. Becker, W. Freude, and J. Leuthold, "Real-time software-defined multiformat transmitter generating 64QAM at 28 GBd," IEEE Photon. Technol. Lett. **22**(21), 1601–1603 (2010).
24. M. Oerder and H. Meyr, "Digital filter and square timing recovery," IEEE Trans. Commun. **36**(5), 605–612 (1988).
25. R. Schmogrow, B. Nebendahl, M. Winter, A. Josten, D. Hillerkuss, S. Koenig, J. Meyer, M. Dreschmann, M. Huebner, C. Koos, J. Becker, W. Freude, and J. Leuthold, "Error vector magnitude as a performance measure for advanced modulation formats," IEEE Photon. Technol. Lett. **24**(1), 61–63 (2012).
26. A. J. Viterbi and A. N. Viterbi, "Nonlinear estimation of PSK-modulated carrier phase with application to burst digital transmission," IEEE Trans. Inf. Theory **29**(4), 543–551 (1983).

1. Introduction

Coherent receivers are key to next generation multi-level polarization-multiplexed modulation formats such as differential quadrature phase-shift keying (PolMUX-DQPSK) [1]. However, coherent detection requires a costly high-quality local oscillator (LO) laser. While coherent detection provides highest sensitivity the price of a narrow linewidth laser is not within reach for many applications such as in metro and access networks. A substitute that does not require a LO would thus be of interest.

Recently, self-coherent detection (SCD) using delay interferometers (DI) has been suggested as a substitute for coherent reception [2–8]. The concept extends self-homodyne differential detection of signals such as the differential phase-shift keying (DPSK) modulation format, where phase differences of zero or 180° are conveyed. SCD schemes do not need an additional laser as a LO, instead the delayed copy of the signal is used for detection. Compared to a coherent receiver that requires digital signal processing (DSP) for carrier phase and frequency estimation, SCD requires advanced DSPs to reconstruct both the phase and the amplitude of the optical field by comparing an actually received complex sample with a previously reconstructed sample. While self-coherent receivers are advantageous with respect to hardware complexity, they mainly suffer from two issues. Firstly, SCD usually shows an optical signal-to-noise ratio (OSNR) penalty compared to coherent receiver. Secondly, SCD has not yet been able to receive a PolMUX signal.

The optical signal-to-noise ratio (OSNR) penalty of SCD compared to coherent receiver is about 2.3 dB [9], due to the fact that the reconstruction process refers to previously estimated symbols which are also noisy. Especially the quantization noise of analog-to-digital converters (ADC) at the receiver is a degrading factor [8]. This OSNR penalty may be reduced with

#172813 - $15.00 USD Received 17 Jul 2012; revised 20 Aug 2012; accepted 21 Aug 2012; published 4 Sep 2012

proper DSP algorithms [2, 8, 10]. These algorithms, which were developed for single polarization, are not directly applicable to self-coherent receivers for PolMUX signals, since the unknown crosstalk between the two polarizations at the receiver strongly distorts the signal constellations. In addition, the fields in the two orthogonal polarizations may destructively interfere at the receiver polarizer yielding zero samples for the reference, causing outages in the reconstruction algorithm operation.

Three principal methods of polarization demultiplexing (PolDEMUX) were mostly developed for differential detection, which can in principle be also applied to SCD. The first method resorts to an external polarization controller for manually [11, 12] or automatically aligning the signal to the receiver polarization axis [13–15]. No special signal format is needed. While automatic alignment does not require fast DSP circuits, it relies on high-speed endless polarization controllers. The second method, suitable for return-to-zero (RZ) signals, consists of interleaving the RZ signals propagating in two orthogonal polarizations by introducing a time offset of half symbol duration. At the receiver, the signals are detected using polarization-insensitive decision circuitry operating at twice the symbol rate [16], requiring high-speed photo-detectors and electronics. The third method uses multiple DIs with a variant of the least mean square (LMS) algorithm [17]. In this scheme the authors not only differentially detect the signals in two orthogonal polarizations, but they also cross-couple the two polarizations optically so that the cross product between the two orthogonally polarized signals can be formed by DSP. The advantage is that PolDEMUX occurs at the symbol rate. The disadvantage is the more complex optical circuitry, and the cost for twice as many photodiodes and ADCs, relative to the first SCD method and to a coherent receiver.

Unfortunately, in SCD, post-detection noise accumulates in the field reconstruction recursion, leading to a random-walk process of the complex recovered signal [7, 8] if no preventive measures are taken. Due to the independent noise random walks in the two polarizations, the PolDEMUX algorithms [18] commonly used in coherent detection system are not directly applicable for SCD system.

In this paper, we present a SCD receiver based on the principle that is different from the above methods. It does not require polarization controller, time interleaving, and a doubled set of detectors. We estimate the change of the state of polarization with training sequences, then use decision feedback to reconstruct the field and to mitigate the noise-induced random walk that affects the usual PolDEMUX methods. To address "zero-reference" outages in one polarization, we use the signal in the other polarization to estimate the "lost" reference. To this end, a variation of the PolMUX-DQPSK format is introduced, whereby the constellations in both polarizations are rotated by 45° relative to each other. An experimental demonstration of the SCD dual polarization scheme is presented for 112 Gbit/s PolMUX-DQPSK reception.

2. PolMUX transmission and self-coherent reception

A polarization multiplexed transmission system with a self-coherent receiver is presented in Fig. 1(a). Two equivalent configurations of the self-coherent receiver optical front-end (OFE) are considered: An OFE with two phase-offset delay interferometers (DI) as in Fig. 1(b), and an OFE with an optical hybrid, Fig. 1(c).

The transmission link shown in Fig. 1(a) comprises two sub-transmitters (Tx_x, Tx_y) that carry two independent data streams, S_x and S_y. The signals generated by the two transmitters are orthogonally polarized. Their electric fields are denoted with E_x and E_y. The two signals are superimposed in a polarization beam combiner (PBC) to form the polarization multiplexed (PolMUX) signal, which is transmitted along a fiber, experiencing a random change of the state of polarization (SOP). The channel is modeled as a matrix **C** including arbitrary polarization rotations $\mathbf{R}_n$, arbitrary order of polarization mode dispersion ($\mathbf{PMD}_n$), and arbitrary phase offset **P**, as detailed in Section 2.1. In the polarization diverse self-coherent receiver, the signal is split by a polarization beam splitter (PBS) in two orthogonal linear polarizations, the output fields of which are denoted with E_x' and E_y'. These signals are a mixture of the

#172813 - $15.00 USD Received 17 Jul 2012; revised 20 Aug 2012; accepted 21 Aug 2012; published 4 Sep 2012

transmitted E_x and E_y as generated by the random SOP change along the fiber. Both polarizations are processed in a self-coherent receiver, the optical front-end (OFE) of which can be implemented by either of two following schemes.

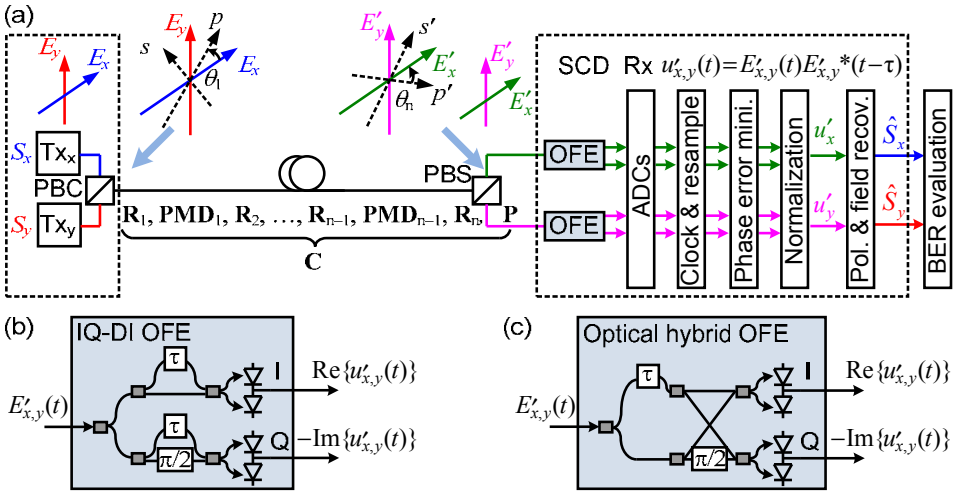

Fig. 1. Polarization multiplexed transmission system with self-coherent receiver (SCD Rx). (a) System schematic with SCD Rx and its DSP modules. Transmitters Tx$_x$ and Tx$_y$ generate two signals E_x and E_y carrying data S_x and S_y, which are then combined in a PBC to form a Pol-MUX signal. In the fiber the signal experiences a random change of the state of polarization described by a matrix (**C**) which consists of arbitrary polarization rotations $(\mathbf{R})_n$, arbitrary order of $\mathbf{PMD}_n$, and arbitrary phase offset (**P**). The signal is then detected in a SCD Rx. There are two options for realizing the optical front-end (OFE) for detecting the in-phase (I) and quadrature phase (Q) signal: (b) OFE with two quadrature phase-offset DIs (IQ-DI) (c) OFE with optical hybrid.

Delay interferometer front-end. In Fig. 1(b) two DIs with balanced detectors are shown. The input of each DI is either $E'_x(t)$ or $E'_y(t)$, denoted by $E'_{x,y}(t)$ for short. Within each DI, the complex signal $E'_{x,y}(t)$ is mixed with its delayed copy $E'_{x,y}(t-\tau)$. By carefully choosing the excess phase difference between the two arms, either an in-phase component $\mathrm{Re}\{u'_{x,y}(t)\} = \mathrm{Re}\{E'_{x,y}(t)E'^{*}_{x,y}(t-\tau)\}$ (I, zero phase difference, upper arm in Fig. 1(b)) or a quadrature phase signal $-\mathrm{Im}\{u'_{x,y}(t)\} = -\mathrm{Im}\{E'_{x,y}(t)E'^{*}_{x,y}(t-\tau)\}$ (Q, $\pi/2$ phase difference, lower arm in Fig. 1(b)) is detected by the balanced photodiode pair. We write the operation performed by the DI together with the balanced detector mathematically as

$$u'_{x,y}(t) = E'_{x,y}(t)E'^{*}_{x,y}(t-\tau). \tag{1}$$

The derivation of the equation can be found in Appendix A.

Optical hybrid front-end. An equivalent alternative scheme is shown in Fig. 1(c) where a 2 × 4 optical hybrid is used similarly to a coherent receiver. In lieu of the local oscillator, the incoming signal is delayed by τ, and this copy is fed into the 2 × 4 optical hybrid in order to interfere with the original signal. Multiple variations of 2 × 4 optical hybrids exist, implemented by discrete couplers, by star-couplers [19] or by multimode interference couplers [20]. The outputs are identical to the ones of the DI front end.

#172813 - $15.00 USD Received 17 Jul 2012; revised 20 Aug 2012; accepted 21 Aug 2012; published 4 Sep 2012

After the balanced detection in either of the front-ends, the complex quantities u_x' and u_y' are converted into the digital domain using analog to digital converters (ADCs). Digital signal processing (DSP) algorithms are then applied to recover the transmitted signals. At the outputs of the DSP, the demodulated signals $\hat{S}_x$ and $\hat{S}_y$ are available for further evaluation, for instance for a BER measurement. The DSP algorithms include clock recovery, resampling, phase error correction, normalization, polarization and field recovery. These last two functions are the subject of a new algorithm, which is our focus in this paper.

In the remainder of this section we will present a model of the fiber channel, with which we analyze the interference between the Tx_x and Tx_y signals and summarize the challenges that need to solve. At the end, the principle of our transmitter and receiver will be presented.

2.1. Channel model

A polarization multiplexed transmitter with a fiber channel and a polarization diverse SCD receiver is shown in Fig. 1(a). The fiber channel introduces some arbitrary SOP changes so that the detected polarization consists of a mixture between the two transmitted signals.

A possible scenario as of how the SOP may vary when passing from transmitter to receiver is depicted in the upper part of the figure. The quantities E_x and E_y represent the linearly polarized electric field components at the transmitter Tx_x and Tx_y. The two signals are combined at a PBC whose linear eigenstates are aligned with the polarization axes of E_x and E_y (blue and red coordinate systems). After the PBC, a fiber is attached. The fiber is modeled by numerous birefringent slices all of which have a different orientation of the fast and the slow axes and a different PMD. The first slice of the fiber model has linear eigenstates p (**p**arallel) and s (**s**enkrecht, perpendicular), which are rotated by an angle of θ_1 with respect to E_x and E_y. The signals have to be remapped to a new coordinate system. This operation can be described by a Jones matrix $\mathbf{R}_1$. The last slice of the fiber model has linear eigenstates p' and s'. At the end of the fiber a PBS with linear polarization eigenstates E_x' and E_y' projects this electric field on its eigenstates (green and magenta coordinate system), and in addition introduces a phase offset $\delta\phi_{\mathrm{PBS}}$ between the two signals. This phase offset is modeled by a matrix **P** as shown in Eq. (2). The rotation angle between the eigenstates of PBS and last fiber slice is θ_{n}. The coordinate system transformation is described by matrix $\mathbf{R}_{\mathrm{n}}$.

Neglecting the propagator and any loss common to both polarizations, the channel is then described by a unitary Jones matrix **C** [2], which including arbitrary polarization rotations $\mathbf{R}_{\mathrm{n}}$, and arbitrary order of $\mathbf{PMD}_{\mathbf{n}}$, and phase offset **P**,

$$\begin{bmatrix} E_x' \\ E_y' \end{bmatrix} = \begin{bmatrix} C_{11} & C_{12} \\ C_{21} & C_{22} \end{bmatrix} \begin{bmatrix} E_x \\ E_y \end{bmatrix}, \quad \mathbf{C} = \mathbf{P} \cdot \mathbf{R}_{\mathrm{n}} \cdot \mathbf{PMD}_{\mathrm{n}} \cdot \mathbf{R}_{\mathrm{n-1}} \ldots \mathbf{R}_2 \cdot \mathbf{PMD}_1 \cdot \mathbf{R}_1,$$
$$\mathbf{R}_{\mathrm{n}} = \begin{bmatrix} \cos(\theta_{\mathrm{n}}) & \sin(\theta_{\mathrm{n}}) \\ -\sin(\theta_{\mathrm{n}}) & \cos(\theta_{\mathrm{n}}) \end{bmatrix}, \mathbf{PMD}_{\mathrm{n}}(\Delta\omega) = \begin{bmatrix} 1 & 0 \\ 0 & \mathrm{e}^{-\mathrm{j}(\Delta\omega\,\tau_{\mathrm{DGDn}} + \delta\phi_{\mathrm{PMDn}})} \end{bmatrix}, \mathbf{P} = \begin{bmatrix} 1 & 0 \\ 0 & \mathrm{e}^{-\mathrm{j}\delta\phi_{\mathrm{PBS}}} \end{bmatrix}. \tag{2}$$

Here, $\mathbf{PMD}_{\mathrm{n}}$ represents the first-order PMD within the fiber. Assuming a time dependency $\exp(\mathrm{j}\omega t)$ with optical angular frequency ω, the differential phase shift between the two principal states of polarizations in a signal bandwidth $\Delta\omega / (2\pi)$ is $\Delta\omega\,\tau_{\mathrm{DGDn}} + \delta\phi_{\mathrm{PMDn}}$, and the differential group delay is τ_{DGDn}. Additional effects could have been also included.

2.2. Challenges for signal recovery

The original Tx_x and Tx_y signals are undergoing SOP change in the channel. As a consequence the signals from Tx_x and Tx_y are mixed in the receiver. The SCD receiver needs to

#172813 - $15.00 USD Received 17 Jul 2012; revised 20 Aug 2012; accepted 21 Aug 2012; published 4 Sep 2012

recover $\hat{S}_x$ and $\hat{S}_y$ from u'_x and u'_y. This can be done in three steps. The first step is the field recovery that E'_x and E'_y are reconstructed from u'_x and u'_y. The second step is the polarization recovery to recover E_x and E_y from E'_x and E'_y. At the end, it's the demodulation that $\hat{S}_x$ and $\hat{S}_y$ are retrieved from E_x and E_y. There are several challenges that need to be solved for such a SCD receiver.

The first challenge is that the mixing of the two signals could lead to destructive interference to the extent that the signal at the receiver becomes zero. To illustrate this issue we give an example using a PolMUX QPSK signal transmitted in a very simple channel consisting only one fiber slice. In our simple channel illustration we neglect PMD and assume a zero phase offset after the PBS. In this case, the matrices $\mathbf{R}_1$, $\mathbf{PMD}_1$, and $\mathbf{P}$ are all identity matrices. The eigenstates of PBS with matrix $\mathbf{R}_2$ are rotated with respect to the eigenstates of PBC, so that the transmitted field components E_x and E_y are combined to new electric field components E'_x and E'_y along the PBS eigenstates. Here we assume a rotation by $\theta_2 = -45°$, see Fig. 2(a). We find

$$\begin{bmatrix} E'_x \\ E'_y \end{bmatrix} = \frac{1}{\sqrt{2}} \begin{bmatrix} I'_x + \mathrm{j}Q'_x \\ I'_y + \mathrm{j}Q'_y \end{bmatrix} \exp(\mathrm{j}\omega t) = \frac{1}{\sqrt{2}} \begin{bmatrix} 1 & -1 \\ 1 & 1 \end{bmatrix} \begin{bmatrix} E_x \\ E_y \end{bmatrix} = \frac{1}{\sqrt{2}} \begin{bmatrix} E_x - E_y \\ E_x + E_y \end{bmatrix}. \qquad (3)$$

As an example, we assume QPSK where $E_{x,y} \in \frac{1}{\sqrt{2}}\{1+\mathrm{j},\ -1+\mathrm{j},\ 1-\mathrm{j},\ -1-\mathrm{j}\}\exp(\mathrm{j}\omega t)$. By substituting into Eq. (3), we arrive at the constellation diagrams in terms of the real (I, in-phase) and imaginary part (Q, quadrature phase) of the complex envelope of the carrier $\exp(\mathrm{j}\omega t)$, Fig. 2(b). As an issue with the reception scheme one may notice the zeros in the Rx constellation diagrams. The zeros result from a destructive interference between E_x and E_y when carrying identical symbols. These zeros result in outages of the field reconstruction for E'_x and E'_y. Special care need to be taken to overcome this issue (details in Section 2.5).

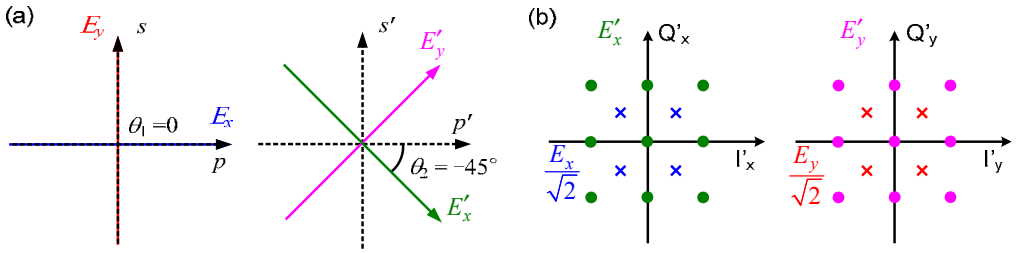

Fig. 2. (a) Illustration of Tx and Rx polarization states. (b) Constellation diagram as sent off by the Tx_x (×) and Tx_y (×) and constellation diagrams as received by the Rx in the two polarizations x' (•) and y' (•) when being sent over the channel in Eq. (2). The two QPSK (×, ×) are mixed and form new constellations $E'_x = (E_x - E_y)/\sqrt{2}$ (•) and $E'_y = (E_x + E_y)/\sqrt{2}$ (•). Zeros in the center of the constellations result from destructive interference.

The second challenge is to avoid error propagation during the field reconstruction process. The error may propagate because the signal is reconstructed using the previous received symbol as a reference. With this a single error could lead to an error in all subsequently reconstructed fields. However, this would not be an issue if the value of the received quantities $S_{x,y}$ would not dependent on the previous detection but only on the difference between two adjacent samples of the field. Therefore, we differentially encoded the transmitter signals. The

#172813 - $15.00 USD Received 17 Jul 2012; revised 20 Aug 2012; accepted 21 Aug 2012; published 4 Sep 2012

transmitter is going to be discussed in the next section and the error propagation will be discussed in more detail in Section 2.5.

The third challenge is to undo the SOP change of the fiber. For this we will introduce a training sequence to estimate the channel matrix **C** in the next section and Appendix B.

2.3. Transmitter with differential encoding and training sequence for channel estimation

The data in the transmitter are differentially precoded (DP) in order to avoid error propagation as outlined in Section 2.2. We start with the complex data sequence $S(n)$ belonging to a certain constellation. By differentially precoding, $S(n)$ is processed into a complex symbols $A(n)$ at discrete times $t_n = n\tau$ at multiples n of the symbol period τ [21],

$$A(n) = S(n)\breve{A}(n-1), \tag{4}$$

where $\breve{A}(n-1)$ retains the same phase as $A(n-1)$, but its magnitude is normalized to one, i. e., $\breve{A}(n-1) = A(n-1)/|A(n-1)|$. If we take standard DQPSK as an example, we have $S(n) \in \{\pm 1, \pm \mathrm{j}\}$. Given the sequence $S(n)$ = [1, j, –1, 1, –j…] and $A(0) = 1$, we get $A(n)$ = [1, j, –j, –j, –1…].

The differentially precoded signal $A(n)$ is then modulated on an optical carrier. In a polarization multiplexed system we convey two signal streams $A_x(n)$ and $A_y(n)$ on the two orthogonal SOP, say, linear polarizations in x and y-direction. The optical signals after the modulation are denoted $E_x = A_x(n)\exp(\mathrm{j}\omega t)$ and $E_y = A_y(n)\exp(\mathrm{j}\omega t)$. The data flow is shown in Fig. 3. In practice, the oscillator is a laser and the mixer is implemented by an optical IQ-modulator.

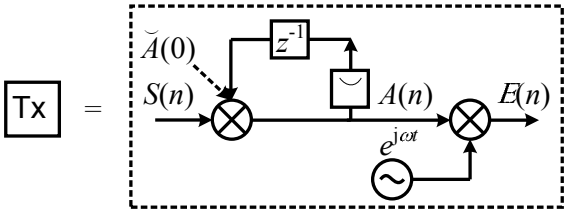

Fig. 3. Schematic drawing of the transmitter. $S(n)$ is differentially encoded into a $A(n)$ by adding $\breve{A}(n-1) = A(n-1)/|A(n-1)|$. The symbol z^{-1} (representing the z-transform) stands for a time delay by one bit. Then the $A(n)$ is modulated on an optical carrier with angular frequency ω. The mixer output is the time sequence $E(n)$.

In the fiber channel, the signals experience an SOP change. Because in our case the optical fields $E'_{x,y}(t)$ cannot be measured directly, but rather $u'_{x,y}(t) = E'_{x,y}(t)E'^{*}_{x,y}(t-\tau)$ after the balanced detectors in Fig. 1(b), conventional polarization demultiplexing does not work, and we need a sequence of training symbols for estimating the channel matrix **C** which is determined by 4 complex quantities C_{ij} (8 real numbers). With known electric field components $E_x = A_x \exp(\mathrm{j}\omega t)$ and $E_y = A_y \exp(\mathrm{j}\omega t)$ and measured fields E'_x and E'_y, four values of $A_{x,y}$ in each polarization would suffice for uniquely calculating **C**. However, we measure only the quantities $u'_{x,y}(t) = E'_{x,y}(t)E'^{*}_{x,y}(t-\tau)$, and therefore only phase differences can be determined. As a consequence, the estimated complex channel matrix coefficients $\hat{C}_{11}$ and $\hat{C}_{12}$ share a common undetermined phase factor so that only their phase difference is known. The same is true for $\hat{C}_{21}$ and $\hat{C}_{22}$. This does not affect the channel estimation (see Appendix B), but the number of determinable real quantities is reduced to 6. Therefore a minimum of three transitions per polarization has to be evaluated, leading to a minimum symbol number of 4. Longer symbol sequences could be employed to estimate **C** by minimizing the least-mean-square error for the matrix coefficients. For demonstrating the concept, we use the minimum

#172813 - $15.00 USD Received 17 Jul 2012; revised 20 Aug 2012; accepted 21 Aug 2012; published 4 Sep 2012

training symbol length consisting of a preamble (0, 1, 1) and two groups of 4 complex symbols with three valid transitions for each polarization,

$$\begin{array}{l|llll|l} A_x(1...8):\ldots & 0 & 1 & 1 & 1 & 1 & 0 & 0 & A_x(8)\ldots \\ \hline A_y(1...8):\ldots & 0 & 1 & 1 & 0 & 0 & 1 & 1 & A_y(8)\ldots \end{array}. \tag{5}$$

Any symbol from the transmitted constellation can be chosen for the symbols $A_x(8)$ and $A_y(8)$, which are used to start the field recovery algorithm. The preamble starting with the two zeros in the two polarizations serves as a uniquely identifiable symbol sequence which must not be part of the transmitted constellation. Appendix B provides details of the channel estimation.

2.4. Self-coherent receiver with decision feedback

The receiver recovers the transmitted information $S_{x,y}(n)$. The OFE of the self-coherent receiver processes the transmitted signal $E'_{x,y}(n)$ in polarization x' or y' by interfering them with their delayed copy as shown in Fig. 1. For simplicity, we replaced the SCD Rx, i.e. the mixed analog-digital circuit of the Rx (in Fig. 1) by an equivalent digital circuit (see Fig. 4). In Fig. 4, we take it for granted that a DSP unit transforms the analog inputs $E'_{x,y}(t)$ at sampling times $t = t_n = n\tau$ into digital quantities $E'_{x,y}(n)$.

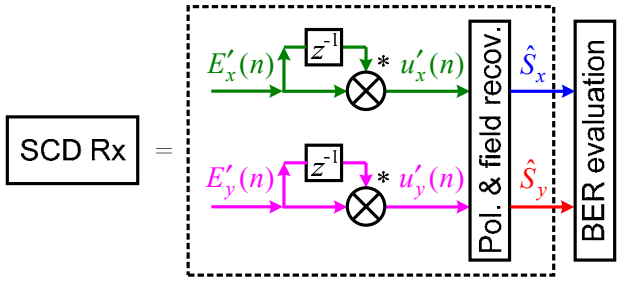

Fig. 4. Equivalent digital representation of the self-coherent detection receiver (SCD Rx). The received signal $E'_{x,y}(n)$ is combined with its conjugated delayed copy that generates $u'_{x,y}(n)$. The symbol z^{-1} (representing the z-transform) stands for a time delay by one bit.

If the SOP does not change, it is $E'_{x,y}(n) = E_{x,y}(n)$ and $u'_{x,y}(n) = u_{x,y}(n)$. After differential decoding we find

$$\begin{aligned} u'_{x,y}(n) = u_{x,y}(n) &= E_{x,y}{}^*(n-1)E_{x,y}(n) = A_{x,y}{}^*(n-1)A_{x,y}(n) \\ &= A_{x,y}{}^*(n-1)S_{x,y}(n)\breve{A}_{x,y}(n-1) = \left|A_{x,y}(n-1)\right|S_{x,y}(n), \end{aligned} \tag{6}$$

where x^* denotes the complex conjugate of quantity x. It should be noted that $|A_{x,y}(n-1)| = 1$ can be chosen for signals $S_{x,y}(n)$ with constant modulus such as for DQPSK. Looking at Eq. (6) we see that with this normalization $u_{x,y}(n) = S_{x,y}(n)$, which means an ideal DQPSK detection. No polarization and field recovery algorithm is needed.

#172813 - $15.00 USD Received 17 Jul 2012; revised 20 Aug 2012; accepted 21 Aug 2012; published 4 Sep 2012

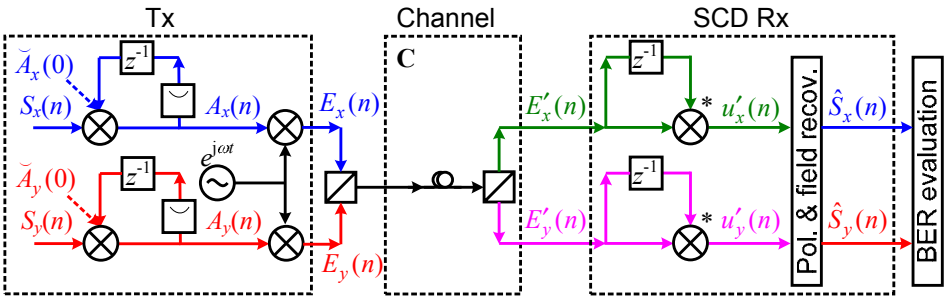

Fig. 5. Equivalent digital representation of the PolMUX signal transmission system. A PolMUX signal E_x and E_y carries encoded symbols of S_x and S_y. After the channel transmission, the receiver projects the signals on new polarization axes which results in E'_x and E'_y. In the SCD Rx, the signal interferes with its delayed copy generating quantities u'_x and u'_y. After polarization and field recovery the transmitted symbols S_x and S_y are recovered and sent for further evaluation.

When the signal is transmitted through a non-ideal channel, polarization crosstalk may occur. Instead of $u'_{x,y}(n) = u_{x,y}(n)$ we receive

$$\begin{aligned} u'_x(n) &= E'^*_x(n-1)E'_x(n), \\ u'_y(n) &= E'^*_y(n-1)E'_y(n), \end{aligned} \tag{7}$$

where E'_x and E'_y are the received fields for polarizations x and y, as described by the channel model of Eq. (2). The overall system is represented by the equivalent digital scheme in Fig. 5.

At the receiver we measure u'_x and u'_y from which we want to recover the transmitted symbols S_x and S_y. However, these symbols are no longer simply obtained at the two DI outputs, due to polarization mixing. The challenge is to recover the fields $E'_x(n)$, $E'_y(n)$ and to perform polarization demultiplexing.

In a first step we need to derive E'_x and E'_y iteratively from the outputs u'_x and u'_y of the self-coherent receiver OFE. A recursive algorithm for single polarization field reconstruction alike to the one displayed in Fig. 6(a) was recently proposed in [8]. Ideally, if we were to know an estimate $\hat{E}'_{x,y}(n-1)$ of the true symbol $E'_{x,y}(n-1)$, we easily could derive an estimate of the following symbol $E'_{x,y}(n)$ by solving the equation $u'_{x,y}(n) = E'^*_{x,y}(n-1)E'_{x,y}(n)$ for the unknown $E'_{x,y}(n)$,

$$\hat{E}'_x(n) = u'_x(n) \big/ \hat{E}'^*_x(n-1), \qquad \hat{E}'_y(n) = u'_y(n) \big/ \hat{E}'^*_y(n-1). \tag{8}$$

The "hat" symbol $\hat{x}$ denotes an estimate of x. By repeatedly applying Eq. (8) we can recursively recover the signal field at sampling times t_n once we have an initial estimate $\hat{E}'_{x,y}(0)$.

In the second step a CMA (constant modulus algorithm) or decision directed LMS equalizer [18] can be applied for polarization demultiplexing same as in a coherent receiver. Once we know $\hat{E}_{x,y}(n)$, the symbols $\hat{S}_x$ and $\hat{S}_y$ are retrieved by differential detection, similarly to Eq. (6). The only change against Eq. (6) is that $\hat{E}_{x,y}(n-1)$ can now be normalized to one, because we are in the digital domain. Thus we directly obtain S_x and S_y,

#172813 - $15.00 USD Received 17 Jul 2012; revised 20 Aug 2012; accepted 21 Aug 2012; published 4 Sep 2012

$$\hat{S}_x(n) = \breve{\hat{E}}_x^*(n-1)\hat{E}_x(n) = \breve{A}_x^*(n-1)S_x(n)\breve{A}_x(n-1) = S_x(n),$$
$$\hat{S}_y(n) = \breve{\hat{E}}_y^*(n-1)\hat{E}_y(n) = \breve{A}_y^*(n-1)S_y(n)\breve{A}_y(n-1) = S_y(n). \quad (9)$$

This equation indicates that $S_x(n)$ and $S_y(n)$ may be derived for any differentially encoding modulation format including QAM, and not only for constant-modulus signals.

However, the recursive algorithm in Eq. (8) has an issue with noise accumulation, because the signals are derived from the previous ones. The recovered field is perturbed by random walk-like noise. This leads to erroneous estimates even after a small number of samples [7, 8]. Even without considering the analytic details, it is evident that as both $u'_{x,y}(n)$ and $\hat{E}'^*_{x,y}(n-1)$ are noisy, their ratio $\hat{E}'_{x,y}(n)$ is even noisier. Such independent noise random walks in the two polarizations make the PolDEMUX algorithms fail. To reduce the noise accumulation, training sequence is used in [8] to monitor the random walk and reset the field recovery when the random walk goes beyond the limit. This method significantly reduces the random walk, however cannot be simply applied for the polarization multiplexed signal because the training sequence can be strongly distorted due to polarization mixing. It also costs extra redundancy.

Another issue of the recursive algorithm in Eq. (8) is that because the initial estimate $\hat{E}'_{x,y}(0)$ is randomly chosen, the estimation can be wrong by a factor of $g = \hat{E}'_{x,y}(0)\big/E'_{x,y}(0)$. As a result, the odd sub-sequence would be scaled by $1/g^*$, $\hat{E}'_{x,y}(1,3,5\ldots) = E'_{x,y}(1,3,5\ldots)\big/g^*$, and the even sub-sequence would be scaled by g, $\hat{E}'_{x,y}(2,4,6\ldots) = gE'_{x,y}(2,4,6\ldots)$. The even and odd sub-sequences of the reconstructed signal would experience different scaling that need be rescaled afterwards [8].

In this paper we advance [8] by improving the reconstruction algorithm, mitigating the noise accumulation problem by means of a special decision feedback, see Fig. 6(b). The key idea is to avoid the use of the previous (noisy) symbol estimate $\hat{E}'_{x,y}(n-1)$ for computing the next one $\hat{E}'_{x,y}(n)$ as it was done in the Fig. 6(a). Instead, we perform the PolDEMUX first by multiplying the result with the inversion of the channel matrix **C**, and then make a decision $\tilde{E}_{x,y}(n)$ for the actual symbol thereby cleaning it from any noise. We then redo the PolMUX by multiplying $\tilde{E}_{x,y}(n)$ with the channel matrix **C** and introducing a delay by one bit. The resulting $\tilde{E}'_{x,y}(n-1)$ represents a noise-free reference for the next symbol, but can still be slightly inaccurate because of the imperfect channel estimation. However, an accumulation of noise is avoided. To further improve the accuracy of the channel estimation and to adapt to the channel variation over time it is possible to use the CMA or decision directed LMS equalizer [18] to adaptively adjust the channel matrix **C**. During the channel estimation, the initial symbols $A_{x,y}(8)$, which are translated into transmitted field quantities $E_{x,y}(8)$, lead us to the values of $\hat{E}'_{x,y}(8)$ as described in Appendix B. Thus $\hat{E}'_{x,y}(8)$ are used as the initial estimate for field reconstruction. At the end $\tilde{E}_{x,y}(n)$ are sent to differential decoder to retrieve $\hat{S}_{x,y}(n)$ same as in Eq. (9).

#172813 - $15.00 USD Received 17 Jul 2012; revised 20 Aug 2012; accepted 21 Aug 2012; published 4 Sep 2012

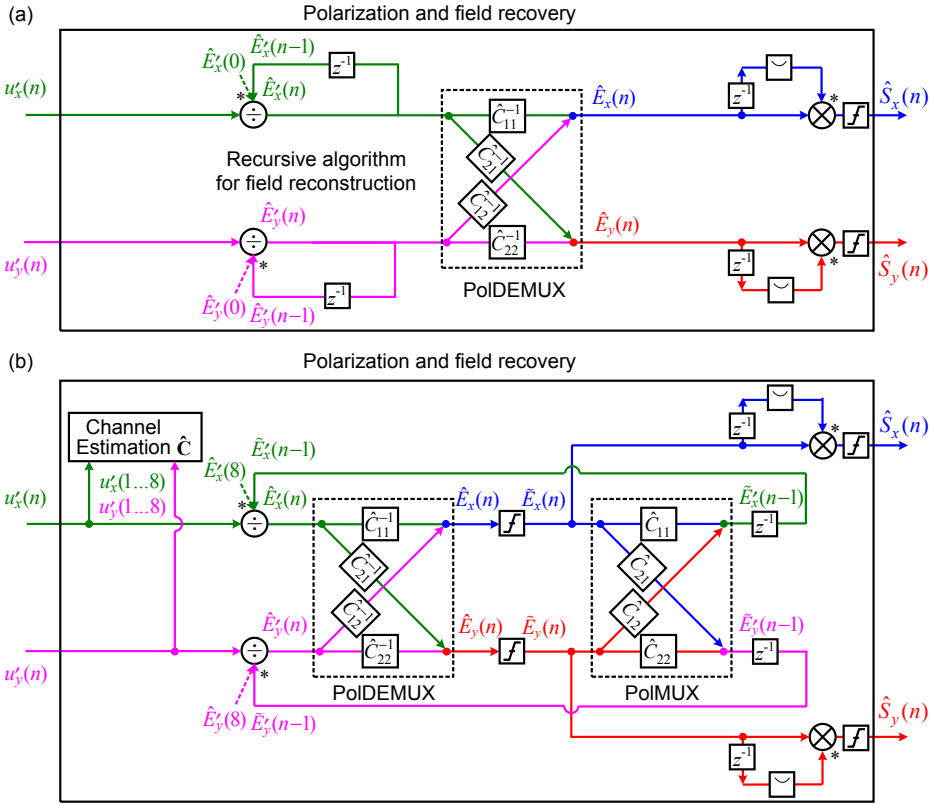

Fig. 6. Polarization and field recovery algorithm to derive the symbol S_x and S_y from complex signal $u'_{x,y}(n)$. (a) The conventional field recovery algorithm using solely Eq. (8). The recovered fields $\hat{E}'_{x,y}(n)$ are then sent to polarization demultiplexing (PolDEMUX) algorithm and differential decoder to retrieve S_x and S_y. This algorithm fails when there is noise accumulation. (b) New polarization and field recovery algorithms. It first performs the PolDEMUX, then uses decision circuits to remove noise. The 'clean' signal $\tilde{E}_{x,y}(n)$ is then multiplied with SOP change to generate the reference $\hat{E}'_{x,y}(n-1)$ for the next field recovery.

2.5. Field outages caused by polarization crosstalk

In extreme cases, when the signals experience strong polarization crosstalk during transmission, one of the two signal polarization states at the receiver could fade due to destructive interference, so that $\hat{E}'_x(n-1)$ or $\hat{E}'_y(n-1)$ become zero. Applying Eq. (8) to recover $\hat{E}'_{x,y}(n)$ will then lead to an infinite output in one of the polarizations, and eventually generate an outage of the field reconstruction process. A non-zero very small value could either be quantized to zero or an inaccurate value could leads to wrong $\hat{E}'_{x,y}(n)$.

To mitigate this problem we modify the field recovery method. We consider a transmitted DQPSK constellation in both polarizations, each constellation may be represented by four phasors $E_{x,y}$ in the x and y-direction, respectively. After transmission, the fields E'_x and E'_y comprise elements with contributions from E_x and E_y. Using Eq. (2) we can express E'_x and E'_y as sum of the respective phasors, i.e. as $E'_x / C_{11} = E_x + (C_{12}/C_{11})E_y$ and $E'_y / C_{22} = E_y + (C_{21}/C_{22})E_x$. For DQPSK where each E_x and E_y has four possible states we get a total of 16 constellation points for E'_x and E'_y, see Fig. 7. If the sub-constellations given by $(C_{12}/C_{11})E_y$ or $(C_{21}/C_{22})E_x$ in Fig. 7(a) and (b) are separated so that different sub-constellations points do not coincide, knowledge of **C** and one polarization state only (i. e. E'_x or E'_y) suffices to identify E'_y and E'_x due to the finite amount of possible states $E'_{x,y}$.

#172813 - $15.00 USD Received 17 Jul 2012; revised 20 Aug 2012; accepted 21 Aug 2012; published 4 Sep 2012

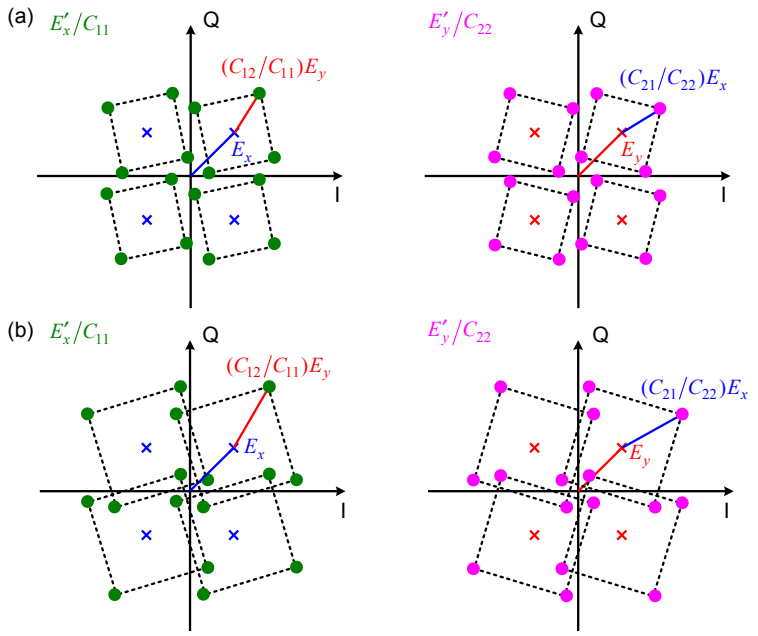

Fig. 7. Examples of PolMUX-DQPSK signal constellation diagrams wherein there is polarization mixing between the two signals. (a), the constellations of E'_x / C_{11} (•) or E'_y / C_{22} (•) have more weight from E_x (×) or E_y (×). (b), E'_x / C_{11} or E'_y / C_{22} have more weight from sub-constellation $(C_{12} / C_{11})E_y$ or $(C_{21} / C_{22})E_x$. Symbol combinations close to zero are detected that might cause outages in the field reconstruction.

However, a second speciality needs to be taken into account. As soon as sub-constellation points coincide, they could result from more than one pair of E_x and E_y. In this case, if for example E'_y cannot be reconstructed due to an outage as in Fig. 2(b), the quantity E'_x cannot be used to uniquely determine E'_y. This problem can be solved by sampling not only the data points, but also halfways during the transition from one symbol to the next, i. e. by a twofold oversampling. For example, in the constellation diagram Fig. 8, the field E'_y transits from point $E'_y(1) \hat{=} 1_y$ (marked with dashed circle) to $E'_y(2) \hat{=} 2_y$ in the center of the constellation, so the next value $E'_y(3)$ could not be recovered because $E'_y(2) = 0$ holds. Therefore we have to rely on the information E'_x only. However, $E'_x(3) = [E_x(3) - E_y(3)] / \sqrt{2} = -1$ from Eq. (3) could result from either $E_x(3) = (-1 + \mathrm{j}) / \sqrt{2}$ and $E_y(3) = (1 + \mathrm{j}) / \sqrt{2}$, or, alternatively, from $E_x(3) = (-1 - \mathrm{j}) / \sqrt{2}$ and $E_y(3) = (1 - \mathrm{j}) / \sqrt{2}$. This ambiguity can be resolved by a twofold oversampling. If it is as assumed above $E'_y(1) \neq 0$ and $E'_y(2) = 0$, then $E'_y(1\tfrac{1}{2}) \neq 0$ would hold, so $E'_y(2\tfrac{1}{2})$ can be calculated with Eq. (8). Depending on the result ($E'_y(2\tfrac{1}{2}) = \pm \mathrm{j} / 2$), we decide on the nearest neighbor $E'_y(3) = [E_x(3) + E_y(3)] / \sqrt{2} = \pm \mathrm{j}$, see Eq. (3). Now the quantities $E_{x,y}(3)$ can be uniquely determined.

#172813 - $15.00 USD Received 17 Jul 2012; revised 20 Aug 2012; accepted 21 Aug 2012; published 4 Sep 2012

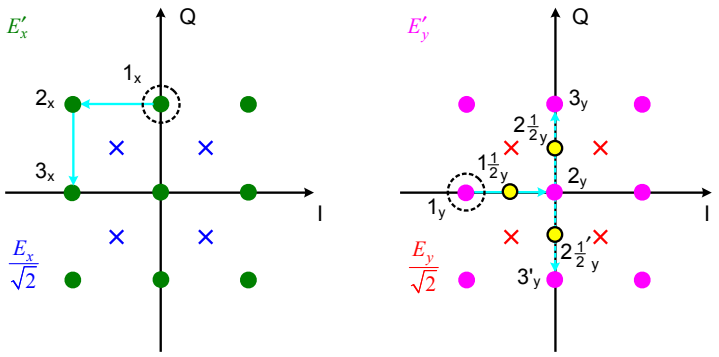

Fig. 8. Example of a PolMUX-DQPSK signal constellations when the linear transformation (**C**) in the fiber consists of an exact –45° rotation. In the constellation of E'_x (•), the signal transits from 1_x to 2_x to the ambiguous point 3_x. In the constellation of E'_y (•), the signal transits from 1_y to 2_y to 3_y or $3'_y$ and the yellow points $1\frac{1}{2}{}_y$, $2\frac{1}{2}{}_y$, and $2\frac{1}{2}{}_y$ are the halfway samples.

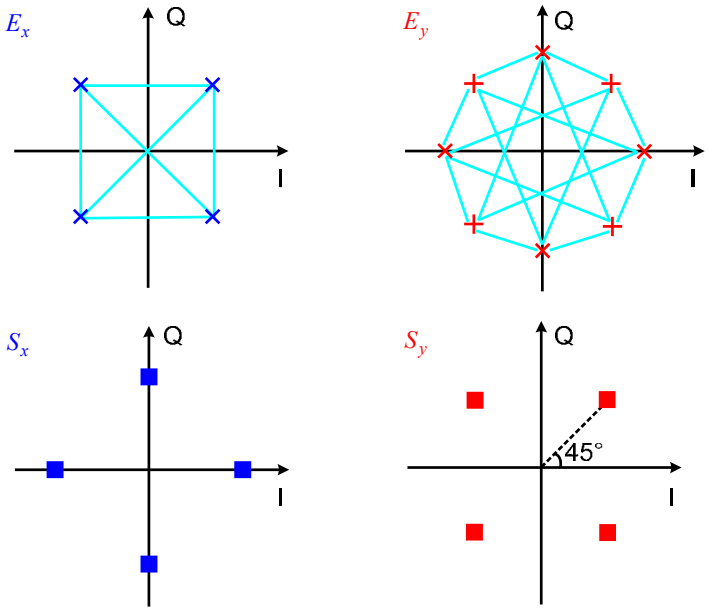

Fig. 9. PolMUX DQPSK signal constellation diagrams. Top row shows the phasor of the signals (E_x and E_y) and their transition lines, the bottom row shows the phasors of the encoded symbols (S_x and S_y) which are also the transitions of the signals (E_x and E_y).

A third special case needs consideration. If two values $E'_y(n)=0$ and $E'_y(n+1)=0$ follow each other, i. e., if no transition takes place, then also $E'_y(n+\frac{1}{2})=0$ is true. As a consequence, $E'_y(n+1\frac{1}{2})$ cannot be recovered so that the oversampling method fails. Therefore such sequences of zeros have to be avoided from the very beginning. To this end, we transmit one of the polarizations, say the y-polarization, with a DQPSK modulation and a progressive 45° phase shift being added for consecutive symbols E_y, Fig. 9 right column. This could be done with an additional clocked phase modulator. The resulting DQPSK phases for the symbols S_y are 45°, 135°, –135° and –45° [22]. The other polarization transmits a normal DQPSK signal with phases 0°, 90°, 180° and –90° for the symbols S_x, Fig. 9 left column. Looking at Fig. 9 and assuming that $E_x(1)=(1+\mathrm{j})/\sqrt{2}$ destructively interferes with $E_y(1)=(1+\mathrm{j})/\sqrt{2}$, none of the 4 possibly following values $E_y(2)=\pm 1,\pm \mathrm{j}$ could destructively interfere with any

#172813 - $15.00 USD Received 17 Jul 2012; revised 20 Aug 2012; accepted 21 Aug 2012; published 4 Sep 2012

of the constellation points $E_x(2) = (\pm 1 \pm \mathrm{j})/\sqrt{2}$. Thus, series of consecutive zeros for $E'_{x,y}$ cannot occur.

Finally, a fourth case needs consideration. If a wrong decision is taken by the decider circuit in Fig. 6(b), the outcome $\tilde{E}_{x,y}(n)$ is erroneous. For a constant modulus DQPSK signal, the wrongly detected field can be written as the correct field times a phase factor, $\tilde{E}_{x,y}(n) = E_{x,y}(n)\exp(\mathrm{j}\varphi^{\varepsilon}_{x,y})$, where $\exp(\mathrm{j}\varphi^{\varepsilon}_{x,y}) \in \{\pm 1, \pm \mathrm{j}\}$. This error carries over to the next reference for the field recovery step $\tilde{E}'_x(n-1) = \exp(\mathrm{j}\varphi^{\varepsilon}_x)\hat{C}_{11}E_x(n-1) + \exp(\mathrm{j}\varphi^{\varepsilon}_y)\hat{C}_{12}E_y(n-1)$ and $\tilde{E}'_y(n-1) = \exp(\mathrm{j}\varphi^{\varepsilon}_x)\hat{C}_{21}E_x(n-1) + \exp(\mathrm{j}\varphi^{\varepsilon}_y)\hat{C}_{22}E_y(n-1)$. If the polarization crosstalk is small, i. e., if $\hat{C}_{12}, \hat{C}_{21}$ are sufficiently small, the error would not propagate due to the differential phase detection scheme: In Eq. (8) the new field $\hat{E}'_{x,y}(n)$ has the same phase factor $\angle\left(1/\hat{E}'_{x,y}{}^{*}(n-1)\right) \propto \angle\hat{E}'_{x,y}(n-1)$ as for the previous field estimate, and differential phase detection then removes this error. However, if polarization crosstalk is strong, the generally different erroneous phase factors from both polarizations appear in mixed form and do not cancel out by differential detection. In the unlikely case that the error phases in both polarizations are the same, $\varphi^{\varepsilon}_x = \varphi^{\varepsilon}_y$, the reference fields in both polarizations would be rotated by the same amount, and the situation would be as in the case of weak polarization coupling. However, if $\varphi^{\varepsilon}_x \neq \varphi^{\varepsilon}_y$, the error propagates and leads to very inaccurate estimates $\hat{E}'_{x,y}(n)$. After polarization demultiplexing, large error vectors magnitudes $\left|e_{x,y}(n)\right| = \left|\tilde{E}_{x,y}(n) - \hat{E}_{x,y}(n)\right|$ would then be found after the decision circuit, and the subsequence field recovery would also become faulty. When this happens, we could minimize the error vectors magnitudes by replacing $\hat{E}'_{x,y}(n)$ with a proper choice out of the possible 16 constellation points at each polarization such that the erroneous phases in both polarizations become the same and $\varphi^{\varepsilon}_x = \varphi^{\varepsilon}_y$ holds, a situation which was discussed previously. The *n*th estimates may be still in error, however, after a maximum of two erroneously detected symbols the error propagation stops and the algorithm turns back to normal operation.

3. Experimental setup and results

The experimental setup is depicted in Fig. 10. A 28 GBd NRZ-DQPSK signal is generated by modulating an external cavity laser (wavelength 1550 nm) with two uncorrelated data sequences applied to an IQ-modulator. The data sequences are generated by a software-defined transmitter [23]. To encode the two polarizations with the normal and the progressive-phase DQPSK signal using a single modulator, we use a special polarization multiplexing emulator. A first frame is generated with normal DQPSK symbols. It consists of the training sequence (TS_x) of the first polarization (Section 2.3) and a DQPSK signal with a PRBS sequence of length $2^8 - 1$. We limit the combination of the training sequence and the DQPSK sequence to a frame of 128 symbols. The next frame contains the symbols of the progressive-phase DQPSK signals, which has a constellation diagram with 8 phase states however only 4 possible phase states in one symbol period as discussed in Fig. 9. The frame comprises the training sequence (TS_y) of the other polarization and a PRBS sequence of length $2^8 - 1$ that is offset from the previous PRBS by 10 bits. The frame is limited to 128 symbols as before. Thus after the IQ-modulator, we have a data sequence of adjacent frames for the two polarizations. The DSP in the receiver has to be switched according to the rhythm of the modulation frame exchange.

#172813 - $15.00 USD Received 17 Jul 2012; revised 20 Aug 2012; accepted 21 Aug 2012; published 4 Sep 2012

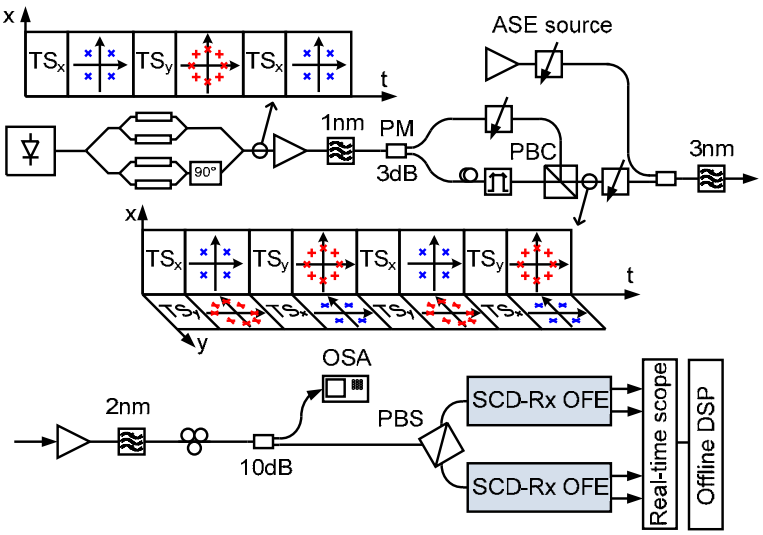

Fig. 10. Experimental setup, the signal is generated in a software defined Tx as a series of frames. In each frame, there is a training sequence ($TS_{x,y}$) for one polarization followed with a DQPSK signal or a progressive-phase DQPSK signal. Then the signal is split and combined in a PBC to form a PolMUX signal. The signal is then experienced with an arbitrary polarization rotation and sent to the self-coherent receiver. An ASE source is used to emulate different OSNR levels.

The signal is then amplified with a polarization maintaining (PM) EDFA and filtered with a 1 nm filter. Then we use a 3dB PM coupler to split the signal onto two arms, where one arm is delayed by 128 symbols with respect to the other one. Both arms are then combined. This yields a 112 Gbit/s bit-aligned PolMUX signal with training sequences for the two polarizations with alternating NRZ-DQPSK and progressive-phase NRZ-DQPSK signal frames. To mimic signals with different OSNR, an amplified spontaneous emission (ASE) noise source has been added. The signal is then filtered with a 3 nm filter and re-amplified before being sent to the self-coherent receiver. At the receiver input we use a 2 nm filter to further suppress the out-of-band noise. A polarization controller emulates polarization rotation in the fiber link. The receiver comprises two pairs of IQ delay interferometers as in Fig. 1(b). The DI delay times equal one symbol duration. After the balanced photo-detectors, the signal is captured by the real-time scope of an Agilent optical modulation analyzer (80 GS/s, 32 GHz bandwidth), which samples the waveforms for off-line processing.

The off-line processing consists of various steps. First, squaring clock recovery algorithm [24] is applied to down-sample the signal to two samples for each in-phase and quadrature phase components of $u'_{x,y}(n)$. Then the signals are normalized and combined to form the complex representations $u'_{x,y}(n)$. After digitally removing the static phase errors in the delay interferometers, we apply our field and polarization recovery algorithm described in Section 2.4. The channel estimation is performed on the first 128 symbols, and afterwards is discontinued, unless it becomes necessary to re-estimate the channel.

We first test the algorithms with low ASE noise. In Fig. 11, we present signal reception under 6 different polarization rotations. Constellation diagrams of the signals $u'_{x,y}(n)$ before performing the polarization recovery algorithms are presented on the left side of each set. Because the signal is repeated with a normal NRZ-DQPSK and a 45° offset NRZ-DQPSK, the constellation resembles an 8PSK format. The zeros in the center are part of the training sequence. During field and polarization recovery, the training sequence is removed from the data and the 45° offset is also canceled. The estimated $\hat{E}_{x,y}$ -constellations after field and

#172813 - $15.00 USD Received 17 Jul 2012; revised 20 Aug 2012; accepted 21 Aug 2012; published 4 Sep 2012

polarization recovery are shown on the right side of each set. The recovered signals' error vector magnitude (EVM) are all below 16%, corresponding to BER less than 10^{-9} [25].

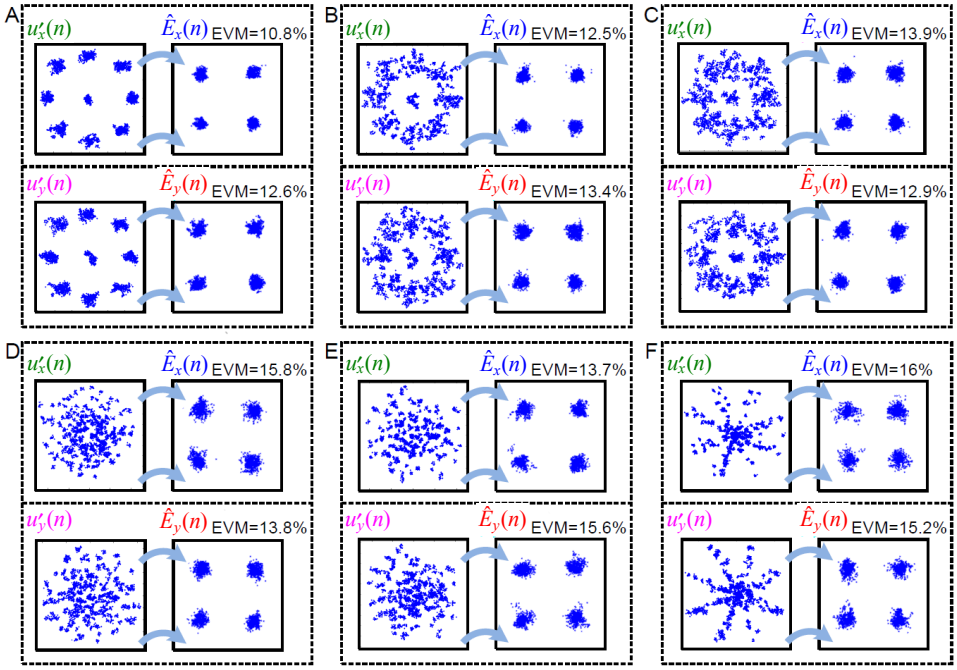

Fig. 11. Constellation diagrams of detected signals $u'_{x,y}$ in x and y polarizations together with the recovered symbols $\hat{E}_{x,y}$ for 6 different polarization states. All measurements were performed at low ASE noise, and 3072 symbols were evaluated.

We then tested the algorithms for different OSNR values and polarization states with and without field and polarization recovery algorithm, Fig. 12. A maximal recording time of 350 μs (98×10^5 symbols) has been used for the BER evaluation. For polarization states 'D' and 'E', the BER at OSNR 16dB is anomalously high. This could be due to the failure of the clock recovery algorithm at low OSNR.

For comparison, we detected the polarization-aligned signal with both a homodyne coherent receiver (black symbols) and with the self-coherent receiver (red symbols). For the signals detected with the homodyne receiver we applied a Viterbi-Viterbi algorithm [26] to correct the phase drift of the local oscillator.

To test the SCD receiver with increasing ASE the same 6 different polarization rotations have been tested as above. When the polarization is aligned, we get the best performance – with and without polarization recovery. The result is virtually same to the one from the coherent receiver. Theoretically, the coherent receiver should provide a result that is about 2.3 dB better than with the differential detection scheme [9]. However, our coherent receiver is not ideal, and other researchers reported similar performance at almost the same symbol rate [1].

It can be seen that our novel algorithm substantially improves the self-coherent detection scheme. While the signal cannot be recovered for a 45° polarization rotation ((F) in Fig. 11 and Fig. 12) without our algorithm, the signal can be recovered with the recovery algorithm in any polarization state.

When the polarization crosstalk is strong we observe an OSNR penalty. This could be due to the fact that the recovered signal is calculated with the signal on two polarizations therefore noise from two sources contributes to the signal: The larger the polarization crosstalk, the

#172813 - $15.00 USD Received 17 Jul 2012; revised 20 Aug 2012; accepted 21 Aug 2012; published 4 Sep 2012

higher the noise penalty. When there are (close) zeros at one polarization, the demodulation is then based on the other polarization which comprises 16 symbol constellation points. This also introduces a higher OSNR penalty to the signal. We should also consider the limitation of the equipment used in the experiment, i.e. the sampling rate and bandwidth of the real-time scope is not sufficient to fully track the transitions of the signal. Therefore the method described in Section 2.5 can only operate with limited efficiency.

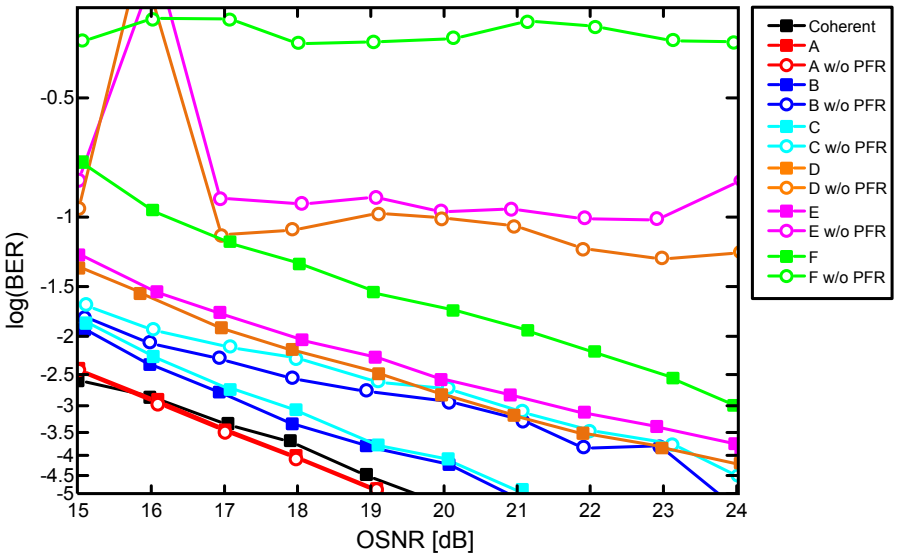

Fig. 12. BER versus OSNR plots of self-coherent receiver for 6 different polarization states with polarization and field recovery (PFR) algorithm (solid symbols) and without PFR algorithm (empty symbols). The black curve shows the OSNR versus BER for a coherent receiver.

4. Conclusion

We presented a self-coherent receiver operating without an external polarization controller. The self-coherent front-end consists of a pair IQ delay interferometers, or it uses a conventional optical hybrid with the LO replaced by a delayed version of the received light for each of the two polarizations. The DSP features a new algorithm based on training sequences to estimate the change of the state of polarization, and a decision feedback to mitigate the noise-driven random walk of the recovered field. The concept was tested for a PolMUX-DQPSK modulation wherein one polarization transmits a normal DQPSK signal, while the other one transmits a progressive-phase DPQSK signal. We experimentally demonstrated that this self-coherent receiver is capable of demultiplexing signals with arbitrary polarizations. In particular, we successfully tested the scheme on an 112Gbit/s PolMUX-DQPSK signal under different polarization states at different OSNR levels.

Appendix A: Signal processing of $E(t)$ by delay interferometers

In this section we derive the mathematical operation performed by two DIs (Fig. 1(b)) onto a signal sequence $E(t)$.

The self-coherent receiver basically comprises two DIs with photo detectors at the constructive and destructive output ports. The operations performed by a single DI onto a signal $E(t)$ therefore given at the constructive and destructive ports are

#172813 - $15.00 USD Received 17 Jul 2012; revised 20 Aug 2012; accepted 21 Aug 2012; published 4 Sep 2012

$$E_{out1}(t) = E(t) + E(t-\tau),$$
$$E_{out2}(t) = E(t) - E(t-\tau). \tag{10}$$

In the photodiodes the fields are converted into photo currents that are proportional to the square of the field magnitude,

$$\begin{aligned} I_{out1}(t) &\propto \left|E(t) + E(t-\tau)\right|^2 \\ &\propto \left|E(t)\right|^2 + \left|E(t-\tau)\right|^2 + 2\left|E(t)\right|\left|E(t-\tau)\right|\cos(\angle E(t) - \angle E(t-\tau)), \\ I_{out2}(t) &\propto \left|E(t) - E(t-\tau)\right|^2 \\ &\propto \left|E(t)\right|^2 + \left|E(t-\tau)\right|^2 - 2\left|E(t)\right|\left|E(t-\tau)\right|\cos(\angle E(t) - \angle E(t-\tau)), \end{aligned} \tag{11}$$

where $\angle x$ denotes the phase of a complex quantity x. After the balanced photodiode receiver, the differential output current is

$$I_{\mathrm{BR}}(t) = I_{out1}(t) - I_{out2}(t) \propto \left|E(t)\right|\left|E(t-\tau)\right|\cos(\angle E(t) - \angle E(t-\tau)). \tag{12}$$

This operation is performed for the in-phase (I in Fig. 1(b)) as well as for the quadrature phase DI (Q in Fig. 1(b)). Because of the π/2 phase offset, the photocurrents $I_{\mathrm{BR}}^{(\mathrm{I})}$ and $I_{\mathrm{BR}}^{(\mathrm{Q})}$ are

$$\begin{aligned} I_{\mathrm{BR}}^{(\mathrm{I})}(t) &\propto \left|E(t)\right|\left|E(t-\tau)\right|\cos(\angle E(t) - \angle E(t-\tau)), \\ I_{\mathrm{BR}}^{(\mathrm{Q})}(t) &\propto \left|E(t)\right|\left|E(t-\tau)\right|\cos(\angle E(t) - \angle E(t-\tau) + \frac{\pi}{2}) \\ &\propto -\left|E(t)\right|\left|E(t-\tau)\right|\sin(\angle E(t) - \angle E(t-\tau)). \end{aligned} \tag{13}$$

After digital acquisition we combine the in-phase and quadrature channels in form of a complex signal,

$$\begin{aligned} u(t) &= I_{\mathrm{BR}}^{(\mathrm{I})}(t) - \mathrm{j}\, I_{\mathrm{BR}}^{(\mathrm{Q})}(t) \\ &\propto \left|E(t)\right|\left|E(t-\tau)\right|\cos(\angle E(t) - \angle E(t-\tau)) + \mathrm{j}\left|E(t)\right|\left|E(t-\tau)\right|\sin(\angle E(t) - \angle E(t-\tau)) \\ &\propto \left|E(t)\right|\left|E(t-\tau)\right|\exp\left[\mathrm{j}(\angle E(t) - \angle E(t-\tau))\right] = E(t)E^*(t-\tau). \end{aligned} \tag{14}$$

As the in-phase and quadrature phase signals are normalized in the DSP section, we simplify the notation by writing $u(t) = E(t)E^*(t-\tau)$. Given the signal is sampled at discrete times $t_n = n\tau$, we can also write this equation as $u(n) = E(n)E^*(n-1)$.

Appendix B: Channel estimation with training sequences

The training sequence for the two polarizations is chosen to be

$A_x(1...8)$: …	0	1	1	1	1	0	0	$A_x(8)$…
$A_y(1...8)$: …	0	1	1	0	0	1	1	$A_y(8)$…

(15)

where $A_x(8)$ and $A_y(8)$ can be any symbol from the transmitted constellation. The preamble with a starting zero serves as a uniquely identifiable symbol sequence. For convenience we set

#172813 - $15.00 USD Received 17 Jul 2012; revised 20 Aug 2012; accepted 21 Aug 2012; published 4 Sep 2012

$E_{x,y} = A_{x,y}$, i. e., we omit encoding the symbols onto an optical carrier which does not change our channel estimation process. At the receiver, we have

$$\begin{aligned}\begin{bmatrix} E_x'(n) \\ E_y'(n) \end{bmatrix}_{n=1\ldots8} &= \begin{bmatrix} C_{11} & C_{12} \\ C_{21} & C_{22} \end{bmatrix} \begin{bmatrix} E_x(n) \\ E_y(n) \end{bmatrix}_{n=1\ldots8} \\ &= \left\{ \begin{matrix} \begin{bmatrix} 0 \\ 0 \end{bmatrix}, \begin{bmatrix} C_{11}+C_{12} \\ C_{21}+C_{22} \end{bmatrix}, \begin{bmatrix} C_{11}+C_{12} \\ C_{21}+C_{22} \end{bmatrix}, \\ \begin{bmatrix} C_{11} \\ C_{21} \end{bmatrix}, \begin{bmatrix} C_{11} \\ C_{21} \end{bmatrix}, \begin{bmatrix} C_{12} \\ C_{22} \end{bmatrix}, \begin{bmatrix} C_{12} \\ C_{22} \end{bmatrix}, \begin{bmatrix} C_{11}E_x(8)+C_{12}E_y(8) \\ C_{21}E_x(8)+C_{22}E_y(8) \end{bmatrix} \end{matrix} \right\}. \end{aligned} \tag{16}$$

After reception with the DI and digital acquisition we measure

$$\begin{aligned}\begin{bmatrix} u_x'(n) \\ u_y'(n) \end{bmatrix}_{n=1\ldots8} &= \begin{bmatrix} E_x'^*(n-1)E_x'(n) \\ E_y'^*(n-1)E_y'(n) \end{bmatrix}_{n=1\ldots8} \\ &= \left\{ \begin{matrix} \begin{bmatrix} 0 \\ 0 \end{bmatrix}, \begin{bmatrix} 0 \\ 0 \end{bmatrix}, \begin{bmatrix} (C_{11}+C_{12})^*(C_{11}+C_{12}) \\ (C_{21}+C_{22})^*(C_{21}+C_{22}) \end{bmatrix}, \begin{bmatrix} (C_{11}+C_{12})^*C_{11} \\ (C_{21}+C_{22})^*C_{21} \end{bmatrix}, \\ \begin{bmatrix} C_{11}^*C_{11} \\ C_{21}^*C_{21} \end{bmatrix}, \begin{bmatrix} C_{11}^*C_{12} \\ C_{21}^*C_{22} \end{bmatrix}, \begin{bmatrix} C_{12}^*C_{12} \\ C_{22}^*C_{22} \end{bmatrix}, \begin{bmatrix} C_{12}^*(C_{11}E_x(8)+C_{12}E_y(8)) \\ C_{22}^*(C_{21}E_x(8)+C_{22}E_y(8)) \end{bmatrix} \end{matrix} \right\}. \end{aligned} \tag{17}$$

From the elements in Eq. (17) we use the first four elements as starting delimiter. Also we do not use $u_{x,y}'(8)$ for channel estimation. This reduces the number of equations to 6. This should be sufficient equations to derive the complex channel elements if the absolute value and the absolute phase are not needed

$$\begin{aligned} u_x'(5) &= C_{11}^*C_{11} = |C_{11}|^2, & u_y'(5) &= C_{21}^*C_{21} = |C_{21}|^2, \\ u_x'(6) &= C_{11}^*C_{12}, & u_y'(6) &= C_{21}^*C_{22}, \\ u_x'(7) &= C_{12}^*C_{12} = |C_{12}|^2, & u_y'(7) &= C_{22}^*C_{22} = |C_{22}|^2. \end{aligned} \tag{18}$$

We employ the same notation as in Eq. (4) for the phase factor $\breve{C}$ of a complex quantity C, and the estimation $\hat{\mathbf{C}}$ of the channel matrix $\mathbf{C}$ results from Eq. (18),

$$\begin{aligned} \hat{C}_{11} &= |u_x'(5)|^{\frac{1}{2}} \exp\left(-\mathrm{j}\angle u_x'(6)\right) = C_{11}\exp\left[\mathrm{j}(-\angle C_{12})\right] = C_{11}\breve{C}_{12}^*, \\ \hat{C}_{12} &= |u_x'(7)|^{\frac{1}{2}} = C_{12}\exp\left[\mathrm{j}(-\angle C_{12})\right] = C_{12}\breve{C}_{12}^*, \\ \hat{C}_{21} &= |u_y'(5)|^{\frac{1}{2}} \exp\left(-\mathrm{j}\angle u_y'(6)\right) = C_{21}\exp\left[\mathrm{j}(-\angle C_{22})\right] = C_{21}\breve{C}_{22}^*, \\ \hat{C}_{22} &= |u_y'(7)|^{\frac{1}{2}} = C_{22}\exp\left[\mathrm{j}(-\angle C_{22})\right] = C_{22}\breve{C}_{22}^*. \end{aligned} \tag{19}$$

Compared to the channel matrix $\mathbf{C}$, its estimation $\hat{\mathbf{C}}$ has common phase factors $\breve{C}_{12}^*$ and $\breve{C}_{22}^*$ for its upper and lower rows, respectively.

As a test, we use this estimated channel matrix to recover the transmitted symbols as discussed in Section 2.4. We first define our starting symbols $\hat{E}_x'(8)$ and $\hat{E}_y'(8)$,

#172813 - $15.00 USD Received 17 Jul 2012; revised 20 Aug 2012; accepted 21 Aug 2012; published 4 Sep 2012

$$\begin{bmatrix}\hat{E}'_x(8)\\ \hat{E}'_y(8)\end{bmatrix}=\begin{bmatrix}\hat{C}_{11}E_x(8)+\hat{C}_{12}E_y(8)\\ \hat{C}_{21}E_x(8)+\hat{C}_{22}E_y(8)\end{bmatrix}=\begin{bmatrix}E'_x(8)\breve{C}_{12}*\\ E'_y(8)\breve{C}_{22}*\end{bmatrix}. \tag{20}$$

Substituting this into Eq. (8), we find $\hat{E}'_x(9)$ and $\hat{E}'_y(9)$,

$$\begin{bmatrix}\hat{E}'_x(9)\\ \hat{E}'_y(9)\end{bmatrix}=\begin{bmatrix}u'_x(9)/\hat{E}'_x*(8)\\ u'_y(9)/\hat{E}'_y*(8)\end{bmatrix}=\begin{bmatrix}E'_x(9)\breve{C}_{12}*\\ E'_y(9)\breve{C}_{22}*\end{bmatrix}. \tag{21}$$

Then we multiply this column matrix with the inverse of the estimated channel matrix $\hat{\mathbf{C}}$,

$$\begin{aligned}\begin{bmatrix}\hat{E}_x(9)\\ \hat{E}_y(9)\end{bmatrix}&=\begin{bmatrix}\hat{C}_{11} & \hat{C}_{12}\\ \hat{C}_{21} & \hat{C}_{22}\end{bmatrix}^{-1}\begin{bmatrix}\hat{E}'_x(9)\\ \hat{E}'_y(9)\end{bmatrix}=\frac{1}{\hat{C}_{11}\hat{C}_{22}-\hat{C}_{12}\hat{C}_{21}}\begin{bmatrix}\hat{C}_{22} & -\hat{C}_{12}\\ -\hat{C}_{21} & \hat{C}_{11}\end{bmatrix}\begin{bmatrix}E'_x(9)\breve{C}_{12}*\\ E'_y(9)\breve{C}_{22}*\end{bmatrix}\\ &=\frac{1}{C_{11}C_{22}\breve{C}_{12}*\breve{C}_{22}*-\hat{C}_{12}\hat{C}_{21}\breve{C}_{12}*\breve{C}_{22}*}\begin{bmatrix}C_{22}\breve{C}_{12}*\breve{C}_{22}* & -C_{12}\breve{C}_{12}*\breve{C}_{22}*\\ -C_{21}\breve{C}_{12}*\breve{C}_{22}* & C_{11}\breve{C}_{12}*\breve{C}_{22}*\end{bmatrix}\begin{bmatrix}E'_x(9)\\ E'_y(9)\end{bmatrix}.\end{aligned} \tag{22}$$

After re-arranging terms we find,

$$\begin{aligned}\begin{bmatrix}\hat{E}_x(9)\\ \hat{E}_y(9)\end{bmatrix}&=\frac{1}{C_{11}C_{22}-C_{12}C_{21}}\begin{bmatrix}C_{22} & -C_{12}\\ -C_{21} & C_{11}\end{bmatrix}\begin{bmatrix}E'_x(9)\\ E'_y(9)\end{bmatrix}\\ &=\begin{bmatrix}C_{11} & C_{12}\\ C_{21} & C_{22}\end{bmatrix}^{-1}\begin{bmatrix}C_{11} & C_{12}\\ C_{21} & C_{22}\end{bmatrix}\begin{bmatrix}E_x(9)\\ E_y(9)\end{bmatrix}=\begin{bmatrix}E_x(9)\\ E_y(9)\end{bmatrix}.\end{aligned} \tag{23}$$

Thus, the symbols for $n = 9$ can be correctly recovered. After the decision circuit (which is introduced because of practical reasons), $\hat{E}_x(9)$ and $\hat{E}_y(9)$ are multiplied with the estimated channel matrix to generate the complex symbol reference for the next symbol recovery,

$$\begin{aligned}\begin{bmatrix}\hat{E}'_x(9)\\ \hat{E}'_y(9)\end{bmatrix}&=\begin{bmatrix}\hat{C}_{11} & \hat{C}_{12}\\ \hat{C}_{21} & \hat{C}_{22}\end{bmatrix}\begin{bmatrix}\tilde{E}_x(9)\\ \tilde{E}_y(9)\end{bmatrix}=\begin{bmatrix}\hat{C}_{11}E_x(9)+\hat{C}_{12}E_y(9)\\ \hat{C}_{21}E_x(9)+\hat{C}_{22}E_y(9)\end{bmatrix}\\ &=\begin{bmatrix}\breve{C}_{12}*(C_{11}E_x(9)+C_{12}E_y(9))\\ \breve{C}_{22}*(C_{21}E_x(9)+C_{22}E_y(9))\end{bmatrix}=\begin{bmatrix}E'_x(9)\breve{C}_{12}*\\ E'_y(9)\breve{C}_{22}*\end{bmatrix}.\end{aligned} \tag{24}$$

Repeating the procedure Eqs. (21)-(24), we are then able to reconstruct the subsequent symbols.

There are two extreme cases that cannot be treated with Eq. (19), namely if either of the $u'_{x,y}(5\ldots7)$ is close to zero, i. e., if there is no polarization crosstalk C_{12}, $C_{21} \to 0$, or if the polarization states are interchanged C_{11}, $C_{22} \to 0$,

$$\begin{bmatrix}C_{11} & C_{12}\\ C_{21} & C_{22}\end{bmatrix}=\begin{bmatrix}1 & 0\\ 0 & 1\end{bmatrix}\quad\text{or}\quad\begin{bmatrix}C_{11} & C_{12}\\ C_{21} & C_{22}\end{bmatrix}=\begin{bmatrix}0 & 1\\ 1 & 0\end{bmatrix}. \tag{25}$$

In this case, $u'_{x,y}(6)$ in Eq. (18) becomes very small, and its argument needed in Eq. (19) for calculating $\hat{\mathbf{C}}$ is very inaccurate. Depending on $u'_{x,y}(5\ldots7)$, the starting fields $E'_x(8)$ and $E'_y(8)$ are equal to the transmitted fields $E_x(8)$ and $E_y(8)$, or they are equal to the cross-polarized transmitted fields $E_y(8)$ and $E_x(8)$. The subsequent fields $E_{x,y}(9)$, $E_{x,y}(10)$, ... can then be recovered as described previously.

#172813 - $15.00 USD Received 17 Jul 2012; revised 20 Aug 2012; accepted 21 Aug 2012; published 4 Sep 2012

Acknowledgment

This work is supported by the European Commission's Network of Excellence EuroFOS and Karlsruhe School of Optics and Photonics (KSOP). This work was further supported in part by the OTONES trans-national Piano + EU program and by the Israeli Science Foundation (ISF). We further acknowledge the Open Access Publishing Fund of the Karlsruhe Institute of Technology (KIT). The authors would also like to thank S. Koenig, A. Ludwig, Z. Wang, L. Zhou from KIT, and Dr. B. Nebendahl from Agilent Technology for their support and for helpful discussions.

#172813 - $15.00 USD Received 17 Jul 2012; revised 20 Aug 2012; accepted 21 Aug 2012; published 4 Sep 2012